Supplementary Material

Seafloor alkalinity enhancement as a carbon dioxide removal strategy in the Baltic Sea

Andrew W. Dale[1,†], Sonja Geilert[1‡], Isabel Diercks[1], Michael Fuhr[1], Mirjam Perner[1], Florian Scholz[1‖], Klaus Wallmann[1]

[1] GEOMAR Helmholtz Centre for Ocean Research Kiel, Wischhofstr. 1–3, 24148 Kiel, Germany

[†] Corresponding author: adale@geomar.de

[‡] Now at: Department of Earth Sciences, Utrecht University, Utrecht, The Netherlands.

[‖] Now at: Institute for Geology, Center for Earth System Research and Sustainability, Universität Hamburg, Hamburg, Germany.

Supplementary methods

Boknis Eck model set-up

The model is largely based on previous simulations of Boknis Eck biogeochemistry[1], with the inclusion of calcite dissolution and pH. It is designed to simulate the broad trends in geochemistry measured at this site (Supplementary Figure 5). The following solid and dissolved species are considered:

Solid components: highly reactive (i.e. poorly crystalline) iron (oxyhydr)oxide ($Fe(OH)_3$), crystalline iron (oxyhydr)oxide (Fe_{MR}), iron mono-sulphide (FeS), pyrite (FeS_2), and calcite ($CaCO_3$). The iron phases included in the model are intended to broadly represent the operationally defined fractions from sequential extractions on sediments from Boknis Eck[2].

Dissolved components: oxygen (O_2), nitrate (NO_3^-), biologically-stored nitrate in large sulphur bacteria (bNO_3^-), sulphate (SO_4^{2-}), ferrous iron (Fe^{2+}), total hydrogen sulphide (TH_2S), dissolved inorganic carbon (DIC), protons (H^+), total boron (TB), total ammonia (TNH_3), total phosphate (TPO_4), hydroxyl anion (OH^-), calcium (Ca^{2+}) and methane (CH_4).

The turnover of solids (S_o) and dissolved species (S_d) in Boknis Eck sediment was simulated with the model applying the following mass balance equations:

$$\rho \cdot (1-\varphi) \cdot \frac{\partial S_d}{\partial t} = \frac{\partial}{\partial x}\left(\rho \cdot (1-\varphi) \cdot \left(D_B \cdot \frac{\partial S_d}{\partial x} - u_S \cdot S_d\right)\right) + \rho \cdot (1-\varphi) \cdot \Sigma R_{S_d} \quad (1)$$

$$\varphi \cdot \frac{\partial S_o}{\partial t} = \frac{\partial}{\partial x}\left(\varphi \cdot \left(D_S \cdot \frac{\partial S_o}{\partial x} - u_{pw} \cdot S_o\right)\right) + \varphi \cdot \alpha \cdot (bw[S_o] - S_o) + \varphi \cdot \Sigma R_{S_o} \quad (2)$$

with S_d: content of solid species in dry sediment, S_o: concentration of solutes in pore water, t: time, x: sediment depth, ρ: density of dry solids, φ: porosity, D_B: bioturbation coefficient; α: non-local transport coefficient; bw[S_o]: bottom water value of S_o, u_S: burial velocity of solids; u_{pw}: burial velocity of porewater; R_{Sd}: turnover rates of solid species (mmol kg^{-1} yr^{-1}), R_{So}: turnover rates of dissolved species, D_S: molecular diffusion coefficient of dissolved species in sediment pore water. Solids and solutes are simulated in units of (g g^{-1} dry sed.) and mmol g^{-1}, respectively. The model was solved using the solver for partial differential equations of MATHEMATICA version 12 applying the Method-of-Lines approach. Reactions included in the model, model parameters, constitutive equations and boundary conditions are listed in Supplementary Table 1 – 4.

Equilibrium processes in the model are applied to DIC (CO_2 + HCO_3^- + CO_3^{2-}), TH_2S (H_2S + HS^-), water dissociation (H^+ + OH^-), TB ($B(OH)_3$ + $B(OH)_4^-$), TNH_3 (NH_3 + NH_4^+), and TPO_4 (H_3PO_4 + $H_2PO_4^-$ + HPO_4^{2-} + PO_4^{3-}). We applied the approach of Hoffmann et al.[3] to simulate pH in sediment porewaters, based on total alkalinity (TA, Eq. (5) in main manuscript) as the equilibrium invariant and implicit differential variable to solve for the concentration of protons. The rate of change of TA due to biogeochemical reactions was calculated based on the TA changes listed in Supplementary Table 1. Transport of TA and the other equilibrium invariants (DIC, TH_2S, TB, TNH_3, TPO_4) was determined from the transport fluxes of the individual acid-base species.

Equilibrium concentrations of individual acid-base species were calculated as follows:

$$[CO_3^{2-}] = \frac{K_1 \cdot K_2}{[H^+]^2 + [H^+] \cdot K_1 + K_1 \cdot K_2} \cdot [DIC] \quad (3)$$

$$[HCO_3^-] = \frac{K_1 \cdot [H^+]}{[H^+]^2 + [H^+] \cdot K_1 + K_1 \cdot K_2} \cdot [DIC] \quad (4)$$

$$[CO_2] = \frac{[HCO_3^-] \cdot [H^+]}{K_1} \quad (5)$$

$$[OH^-] = \frac{K_W}{[H^+]} \quad (6)$$

$$[HS^-] = \frac{K_S}{K_S + [H^+]} \cdot [TH_2S] \quad (7)$$

$$[H_2S] = \frac{[H^+]}{K_S + [H^+]} \cdot [TH_2S] \quad (8)$$

$$[NH_3] = \frac{K_N}{K_N + [H^+]} \cdot [TNH_3] \quad (9)$$

$$[NH_4^+] = \frac{[H^+]}{K_N + [H^+]} \cdot [TNH_3] \quad (10)$$

$$[B(OH)_4^-] = \frac{K_B}{K_B + [H^+]} \cdot [TB] \quad (11)$$

$$[B(OH)_3] = \frac{[H^+]}{K_B + [H^+]} \cdot [TB] \quad (12)$$

$$[PO_4^{3-}] = \frac{K_{P1} \cdot K_{P2} \cdot K_{P3}}{[H^+]^3 + [H^+]^2 \cdot K_{P1} + [H^+] \cdot K_{P1} \cdot K_{P2} + K_{P1} \cdot K_{P2} \cdot K_{P3}} \cdot [TPO_4] \quad (13)$$

$$[HPO_4^{2-}] = \frac{K_{P1} \cdot K_{P2} \cdot [H^+]}{[H^+]^3 + [H^+]^2 \cdot K_{P1} + [H^+] \cdot K_{P1} \cdot K_{P2} + K_{P1} \cdot K_{P2} \cdot K_{P3}} \cdot [TPO_4] \quad (14)$$

$$[H_2PO_4^-] = \frac{K_{P1} \cdot [H^+]^2}{[H^+]^3 + [H^+]^2 \cdot K_{P1} + [H^+] \cdot K_{P1} \cdot K_{P2} + K_{P1} \cdot K_{P2} \cdot K_{P3}} \cdot [TPO_4] \quad (15)$$

$$[H_3PO_4] = [TPO_4] - [PO_4^{3-}] - [HPO_4^{2-}] - [H_2PO_4^-] \quad (16)$$

Stoichiometric equilibrium constants listed in Supplementary Table 2 were calculated on the total scale using the functions provided by Millero[4] and Zeebe and Wolf-Gladrow[5], and converted to free scale where appropriate using the method outlined by Zeebe and Wolf-Gladrow[5]. For the sake of computational efficiency, the equilibrium constants in the model are defined at the mean temperature and salinity at Boknis Eck.

Rates of biogeochemical process considered are largely driven by the degradation of POC (Supplementary Table 1). The kinetic constants of the biogeochemical reactions were mostly adjusted to simulate trends in porewater concentrations of solutes, carbonate and solid iron phases in Boknis Eck sediments (Supplementary Figure 2). The rate of organic matter degradation typically decreases with depth in the sediment as it becomes more recalcitrant over time[6]. Following Stolpovsky et al.[7], we used an empirical power law function to parameterize POC mineralization as function of sediment depth, *x*, termed R_{POC}:

$$R_{POC} = 0.5 \cdot (B_1 + x)^{B_2} \quad (17)$$

where B_1 and B_2 define the decrease in POC with sediment depth. Assuming that the rain rate of POC to the seafloor (RR_{POC} in mmol cm^{-2} yr^{-1}) provides an upper limit of the total amount of POC available for degradation, B_1 can be defined as[7]:

$$B_1 = (-2 \cdot (B_2 + 1) \cdot RR_{POC})^{\frac{1}{1+B_2}} \quad (18)$$

The value of B_2 was determined constrained from the porewater data measured at Boknis Eck. We obtained improved fits to the porewater data by adjusting the function slightly so that the POC degradation rate below 8 cm was constant with depth. Pathways of POC remineralization include aerobic respiration, denitrification, sulphate reduction and methanogenesis. The transition from one metabolic pathway to another during POC respiration depends on the relative concentrations of the terminal electron acceptors and kinetic half-saturation concentrations. We obtained realistic simulations of particulate iron contents by assuming that $Fe(OH)_3$ is not involved in POC degradation and is only reduced by sulphidic dissolution. POC remineralization is linked to the solubilization of TNH_3 and TPO_4 through the respective stoichiometric ratios (r_{NC} and r_{PC}).

The rate constant for calcite dissolution (k_{CaDiss}) is multiplied by a temperature-dependency term (f_T, Supplementary Table 3). This scales k_{CaDiss} by a factor of two for a temperature change of 10 °C. This approach was taken to magnify the sensitivity of calcite dissolution to changes in bottom water temperature. Nevertheless, the sensitivity analysis showed that calcite dissolution was relatively insensitive to the seasonal temperature amplitude of Boknis Eck bottom waters compared to the other tested factors (See main manuscript).

Boundary conditions

Constant fluxes (rain rates RR_{Sd}) were applied for solids (S_d) at the upper boundary of the model ($x = 0$):

$$\rho \cdot (1-\varphi) \cdot \left(-D_B \cdot \frac{\partial S_d}{\partial x} + u_S \cdot S_d\right)\Big|_{x=0} = RR_{S_d} \quad (19)$$

whereas constant concentrations corresponding to ambient bottom water (bw) values were used for the solutes (S_o) (Supplementary Table 4):

$$S_o|_{x=0} = bw[S_o] \quad (20)$$

A zero gradient condition was applied at the lower boundary (x = L) for both solids and solutes:

$$\frac{\partial S_o(x,t)}{\partial x}\Big|_{x=L} = 0 \qquad \frac{\partial S_d(x,t)}{\partial x}\Big|_{x=L} = 0 \quad (21)$$

The flux of POC to the seafloor was set equal to the mean annual rate of POC degradation at Boknis Eck (~12 mmol m^{-2} d^{-1})[1]. The flux of calcite prior to artificial calcite addition (0.011 g cm^{-2} yr^{-1}) was adjusted to provide a background steady state content of 3 – 4 wt. %[8]. Note that this is lower than 0.026 g cm^{-2} yr^{-1} calculated from the mass accumulation rate at Boknis Eck and the carbonate content of local till along the German coast (~17 wt.%,) that has been assumed to be deposited there[8]. This discrepancy may be explained by the dissolution of carbonate during transport from the coast to the Boknis Eck deep. Natural calcite dissolution may be higher than predicted by the model especially if the sediment is periodically colonized by cable bacteria that are known to enhance calcite dissolution[9,10]. Further experimental investigations are needed to address this inconsistency.

Fluxes of $Fe(OH)_3$ were calculated based on the mass accumulation rate and total iron content measured after total sediment digestion of sediment samples (C_{Fe} = 3 wt.%, F. Scholz unpublished data). Assuming that 68 % of total deposited Fe is highly reactive[2], a good fit to the solid phase Fe data was obtained (Supplementary Figure 5). This is higher than the mean value of reactive Fe in marine margin sediments (~30 %)[11] and points toward enhanced deposition of reactive iron in the deeper parts of the basin, possibly by a basin Fe shuttle[12-14]. The flux of crystalline iron oxides accounted for 13 % of the total iron flux. Since the measured content of Fe_{MR} shows little change with depth in the sediment[15], this fraction was assumed to be inert. It was included in the model to simulate the extent to which solid phase Fe(III) has been converted to solid phase Fe(II), that is, (FeS + FeS_2)/(FeS + FeS_2 + $Fe(OH)_3$ + Fe_{MR}). The model result (~80 %, Supplementary Figure 5) is in very good agreement with mean observations[15] of 78 % (Supplementary Figure 5). Fluxes of other solid species were set to zero.

Upper boundary conditions of TH_2S, TNH_3, TPO_4, CH_4, and NO_3^-, were fixed at typical bottom water concentrations measured in Boknis Eck. The concentration of bNO_3^- was 150 µM based on previous model results and measured concentrations[1,16]. Concentrations of SO_4^{2-}, Ca^{2+} and TB were scaled to salinity, using mean seawater concentrations[5].

Following Melzner et al.[17], the seasonal changes in bottom water temperature (°C), salinity (-), O_2 (mmol g^{-1}) and pH (-) were approximated as follows (Supplementary Figure 1):

$$bw[T] = T_{mean} - T_{amp} \cdot \cos(2 \cdot \pi \cdot (t + 0.7)) \quad (22)$$
$$bw[S] = S_{mean} - S_{amp} \cdot \cos(2 \cdot \pi \cdot (t + 0.7)) \quad (23)$$
$$bw[O_2] = O_{2\_mean} - O_{2\_amp} \cdot \cos(2 \cdot \pi \cdot (t + 0.3)) \quad (24)$$
$$bw[pH] = pH_{mean} - pH_{amp} \cdot \cos(2 \cdot \pi \cdot (t + 0.3)) \quad (25)$$

The pH was measured on the NBS scale[17]. This was converted to the free scale using Eq. (2) in Ulfsbo et al.[18] and dissociation constants for HSO_4^- and HF[5]. Temperature and salinity changes in the bottom water are assumed to affect the whole sediment column instantaneously. Bottom water TA was calculated from salinity[19]:

$$\mathrm{bw[TA]} = (\mathrm{bw[S]} \cdot 25.3 + 1470) \cdot 10^{-6} \quad (26)$$

The bottom water concentrations (in mol kg^{-1}, pCO_2 in µatm) of other acid-base species were then calculated as:

$$\mathrm{bw[H^+]} = 10^{-\mathrm{bw[pH]}} \quad (27)$$

$$\mathrm{bw[CO_2]} = \frac{\mathrm{bw[TA]} - \mathrm{bw[B(OH)_4^-]} - \mathrm{bw[HS^-]} - \mathrm{bw[NH_3]} - \mathrm{bw[HPO_4^{2-}]} - 2\cdot\mathrm{bw[PO_4^{3-}]} - \mathrm{bw[OH^-]} + \mathrm{bw[H_3PO_4]} + \mathrm{bw[H^+]}}{\frac{K_1}{\mathrm{bw[H^+]}} + 2\cdot\frac{K_1\cdot K_2}{\mathrm{bw[H^+]}^2}} \quad (28)$$

$$\mathrm{bw[OH^-]} = \frac{K_W}{\mathrm{bw[H^+]}} \quad (29)$$

$$\mathrm{bw[CO_3^{2-}]} = \frac{\mathrm{bw[CO_2]}\cdot K_1\cdot K_2}{\mathrm{bw[H^+]}^2} \quad (30)$$

$$\mathrm{bw[HCO_3^-]} = \frac{\mathrm{bw[CO_2]}\cdot K_1}{\mathrm{bw[H^+]}} \quad (31)$$

$$\mathrm{bw[pCO_2]} = 10^6 \cdot \frac{\mathrm{bw[CO_2]}}{K_0} \quad (32)$$

$$\mathrm{bw[HS^-]} = \frac{\mathrm{bw[TH_2S]}\cdot K_S}{K_S + \mathrm{bw[H^+]}} \quad (33)$$

$$\mathrm{bw[H_2S]} = \mathrm{bw[TH_2S]} - \mathrm{bw[HS^-]} \quad (34)$$

$$\mathrm{bw[NH_3]} = \frac{\mathrm{bw[TNH_3]}\cdot K_N}{K_N + \mathrm{bw[H^+]}} \quad (35)$$

$$\mathrm{bw[NH_4^+]} = \mathrm{bw[TNH_3]} - \mathrm{bw[NH_3]} \quad (36)$$

$$\mathrm{bw[PO_4^{3-}]} = \frac{\mathrm{bw[TPO_4]}\cdot K_{P1}\cdot K_{P2}\cdot K_{P3}}{\mathrm{bw[H^+]}^3 + \mathrm{bw[H^+]}^2\cdot K_{P1} + \mathrm{bw[H^+]}\cdot K_{P1}\cdot K_{P2} + K_{P1}\cdot K_{P2}\cdot K_{P3}} \quad (37)$$

$$\mathrm{bw[HPO_4^{2-}]} = \frac{\mathrm{bw[TPO_4]}\cdot K_{P1}\cdot K_{P2}\cdot \mathrm{bw[H^+]}}{\mathrm{bw[H^+]}^3 + \mathrm{bw[H^+]}^2\cdot K_{P1} + \mathrm{bw[H^+]}\cdot K_{P1}\cdot K_{P2} + K_{P1}\cdot K_{P2}\cdot K_{P3}} \quad (38)$$

$$\mathrm{bw[H_2PO_4^-]} = \frac{\mathrm{bw[TPO_4]}\cdot K_{P1}\cdot \mathrm{bw[H^+]}^2}{\mathrm{bw[H^+]}^3 + \mathrm{bw[H^+]}^2\cdot K_{P1} + \mathrm{bw[H^+]}\cdot K_{P1}\cdot K_{P2} + K_{P1}\cdot K_{P2}\cdot K_{P3}} \quad (39)$$

$$\mathrm{bw[H_3PO_4]} = \mathrm{bw[TPO_4]} - \mathrm{bw[PO_4^{3-}]} - \mathrm{bw[HPO_4^{2-}]} - \mathrm{bw[H_2PO_4^-]} \quad (40)$$

$$\mathrm{bw[B(OH)_4^-]} = \frac{\mathrm{bw[TB]}\cdot K_B}{K_B + \mathrm{bw[H^+]}} \quad (41)$$

$$bw[B(OH)_3] = bw[TB] - bw[B(OH)_4^-] \quad (42)$$

Bottom water DIC concentration and the saturation state of calcite are then equal to:

$$bw[DIC] = bw[CO_2] + bw[HCO_3^-] + bw[CO_3] \quad (43)$$

$$bw[\Omega_{Calcite}] = \frac{bw[Ca^{2+}] \cdot bw[CO_3^{2-}]}{K_{sp}} \quad (44)$$

Supplementary references

1. Dale, A. W., Bertics, V. J., Treude, T., Sommer, S., and Wallmann, K. (2013) Modeling benthic-pelagic nutrient exchange processes and porewater distributions in a seasonally hypoxic sediment: evidence for massive phosphate release by Beggiatoa?, Biogeosciences, 10, 629-651.
2. Retschko, A. -K., Vosteen, P., Plass, A., Welter, E., Scholz, F. (2023) Comparison of sedimentary iron speciation obtained by sequential extraction and X-ray absorption spectroscopy. Mar. Chem. 252, 104249, https://doi.org/10.1016/j.marchem.2023.104249.
3. Hofmann, A. F., Meysman, F. J. R., Soetaert, K., and Middelburg, J. J. (2008) A step-by-step procedure for pH model construction in aquatic systems. Biogeosciences 5, 227–251, https://doi.org/10.5194/bg-5-227-2008.
4. Millero, F. J. (1995) Thermodynamics of the carbon dioxide system in the oceans. Geochim. Cosmochim. Acta 59, 661-667.
5. Zeebe, R. and Wolf-Gladrow, D. (2001) CO_2 in Seawater: Equilibrium, Kinetics and Isotopes, Elsevier, Amsterdam.
6. Middelburg, J. J. (1989) A simple ratemodel for organic matter decomposition in marine sediments, Geochim. Cosmochim. Acta, 53, 1577–1581.
7. Stolpovsky, K., A. W. Dale, and K.Wallmann (2015), Toward a parameterization of global-scale organic carbon mineralization kinetics in surface marine sediments. Glob. Biogeochem. Cy., 29, 812–829, doi:10.1002/2015GB005087.
8. Wallmann, K., Diesing, M., Scholz, F., Rehder, G., Dale, A. W., Fuhr, M. and Suess, E. (2022) Erosion of carbonate-bearing sedimentary rocks may close the alkalinity budget of the Baltic Sea and support atmospheric CO2 uptake in coastal seas. Front. Mar. Sci. 9:968069. doi: 10.3389/fmars.2022.968069.
9. Seitaj, D., Schauer, R., Sulu-Gambari, F., Hidalgo-Martinez, S., Malkin, S. Y., Burdorf, L. D. W., Slomp, C. P., and Meysman, F. J. R. (2015) Cable bacteria generate a firewall against euxinia in seasonally hypoxic basins, Proc. Nat. Acad. Sci. USA, 112, 13278-13283.
10. Rao, A. M. F., Malkin, S. Y., Hidalgo-Martinez, S., and Meysman, F. J. R. (2016) The impact of electrogenic sulfide oxidation on elemental cycling and solute fluxes in coastal sediment, Geochim. Cosmochim. Acta, 172, 265-286.
11. Raiswell, R., Canfield, D. E. (1998) Sources of iron for pyrite formation in marine sediments. Am. J Sci. 298, 219-245; DOI: https://doi.org/10.2475/ajs.298.3.219
12. Scholz, F., McManus, J., Sommer, S. (2013) The manganese and iron shuttle in a modern euxinic basin and implications for molybdenum cycling at euxinic ocean margins. Chem. Geol. 355, 56-68.
13. Lenz, C., Jilbert, T., Conley, D. J., and Slomp, C. P. (2015) Hypoxia driven variations in iron and manganese shuttling in the Baltic Sea over the past 8 kyr, Geochem. Geophy. Geosy., 16, 3754–3766, https://doi.org/10.1002/2015GC005960.
14. Gustafsson, E., Hagens, M., Sun, X., Reed, D. C., Humborg, C., Slomp, C. P., and Gustafsson, B. G. (2019) Sedimentary alkalinity generation and long-term alkalinity development in the Baltic Sea, Biogeosciences, 16, 437–456, https://doi.org/10.5194/bg-16-437-2019.
15. Perner, M., Wallmann, K., Adam-Beyer, N., Hepach, H., Laufer-Meiser, K., Böhnke, S., Diercks, I., Bange, H. W., Indenbirken, D., Nikeleit, V., Bryce, C., Kappler, A., Engel, A. and Scholz, F. (2022)

Environmental changes affect the microbial release of hydrogen sulfide and methane from sediments at Boknis Eck (SW Baltic Sea). Front. Microbiol. 13:1096062. doi: 10.3389/fmicb.2022.1096062.
16. Preisler, A., de Beer, D., Lichtschlag, A., Lavik, G., Boetius, A., and Jørgensen, B. B. (2007) Biological and chemical sulfide oxidation in a *Beggiatoa* inhabited marine sediment, ISME J., 1, 341–353.
17. Melzner, F., Thomsen, J., Koeve, W., Oschlies, A., Gutowska, M. A., Bange, H. W., Hansen, H. P., and Kortzinger, A.: Future ocean acidification will be amplified by hypoxia in coastal habitats, Mar. Biol., 160, 1875-1888, 2013.
18. Ulfsbo, A. Hulth, S. and Anderson, L. G. (2011) pH and biogeochemical processes in the Gotland Basin of the Baltic Sea. Mar. Chem. 127, 20 – 30.
19. Beldowski, J., Löffler, A., Schneider, B., Joensuu, L. (2010) Distribution and biogeochemical control of total CO_2 and total alkalinity in the Baltic Sea. J. Mar. Sys. 81:252–259
20. Dale, A. W., Sommer, S., Bohlen, L., Treude, T., Bertics, V. J., Bange, H. W., Pfannkuche, O., Schorp, T., Mattsdotter, M., and Wallmann, K. (2011) Rates and regulation of nitrogen cycling in seasonally hypoxic sediments during winter (Boknis Eck, SW Baltic Sea): sensitivity to environmental variables. Estuar. Coast. Shelf Sci., 95, 12-28.
21. Meysman, F. J. R., Risgaard-Petersen, N., Malkin, S. Y., and Nielsen, L. P. (2015) The geochemical fingerprint of microbial long-distance electron transport in the seafloor, Geochim. Cosmochim. Acta, 152, 122-142.
22. Boudreau, B. P. (1997), Diagenetic Models and Their Implementation, 414 pp., Springer, Berlin.
23. Mattila J; Kankaanpää H; Ilus E (2006) Estimation of recent sediment accumulation rates in the Baltic Sea using artificial radionuclides ^{137}Cs and ^{239,240}Pu as time markers. Bor. Environ. Res. 11, 95–107.
24. Christiansen, C. and Kunzendorf, H. (1998) Datings and sedimentation rate estimations during GOBEX a summary. In Emeis, K.C. and. Struck, U., editors, Gotland Deep Experiment (GOBEX), Status report on investigations concerning benthic processes, sediment formation and accumulation, Meereswissenschaftliche Beriche, Warnemiunde 34, 55-76.
25. Leipe, T., Tauber, F., Vallius, H., Virtasalo, J., Uscinowicz, S., Kowalski, N., Hille, S., Lingdren, S., Myllyvirta, T. (2011). Particulate organic carbon (POC) in surface sediments of the Baltic Sea. Geo-Mar. Lett. 31, 175–188. doi: 10.1007/s00367-010-0223-x.
26. Noffke, A., Sommer,S., Dale, A. W., Hall, P. O. J., Pfannkuche, O. (2016) Benthic nutrient fluxes in the Eastern Gotland Basin (Baltic Sea) with particular focus on microbial mat ecosystems. J. Mar. Sys. 158, 1–12.
27. Stockenberg, A. and Johnstone, R. W. (1997) Benthic denitrification in the Gulf of Bothnia. Estuar. Coast. Shelf Sci. 45, 835–843.

Supplementary figures

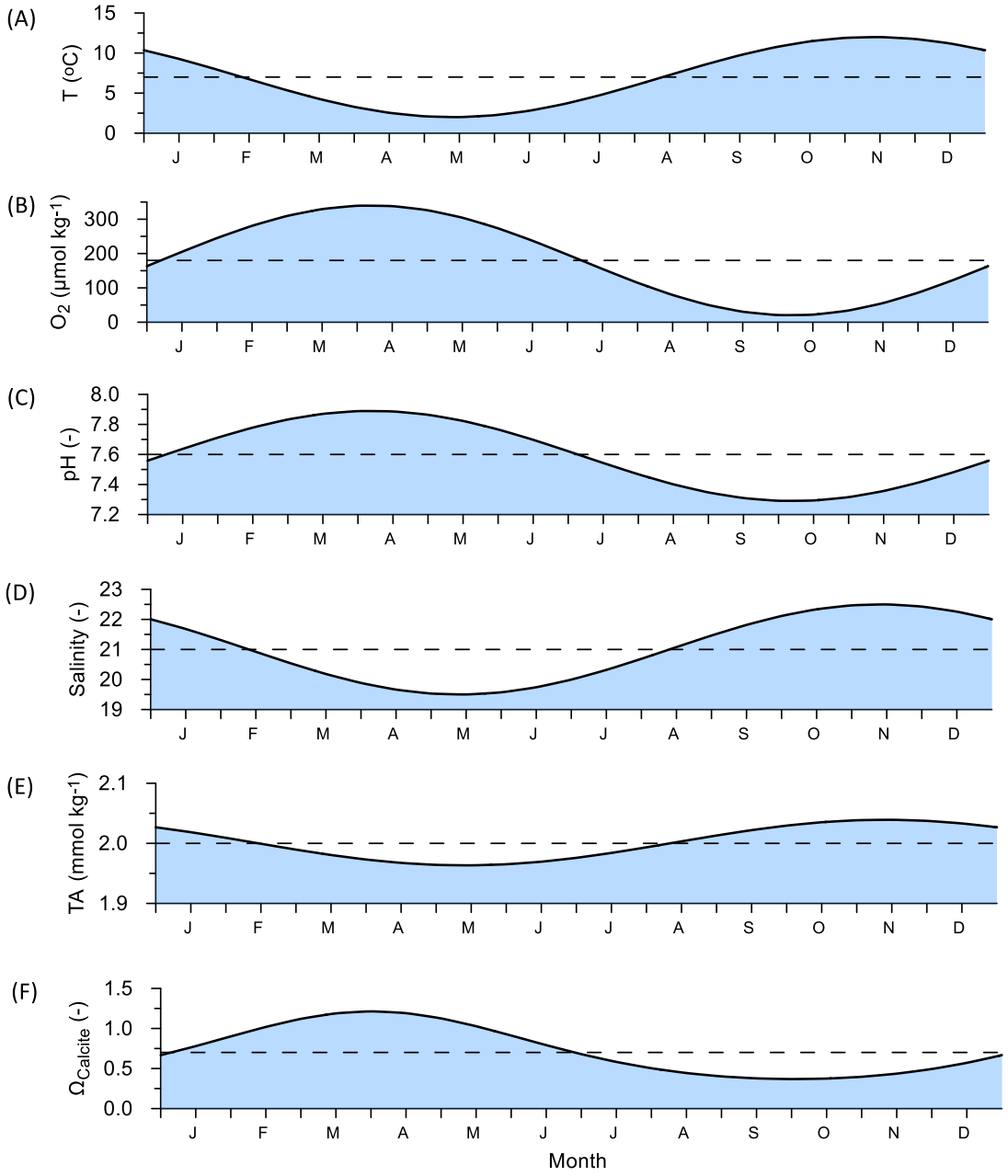

***Supplementary Figure 1**. Seasonal cycle of bottom water forcing functions used as seafloor boundary conditions in the model. (A) Temperature, (B) dissolved oxygen, (C) pH (free scale), (D) total alkalinity, (E) salinity, and (F) calcite saturation. Horizontal dashed lines show the mean annual values. The seasonal trends are based on measured data[17].*

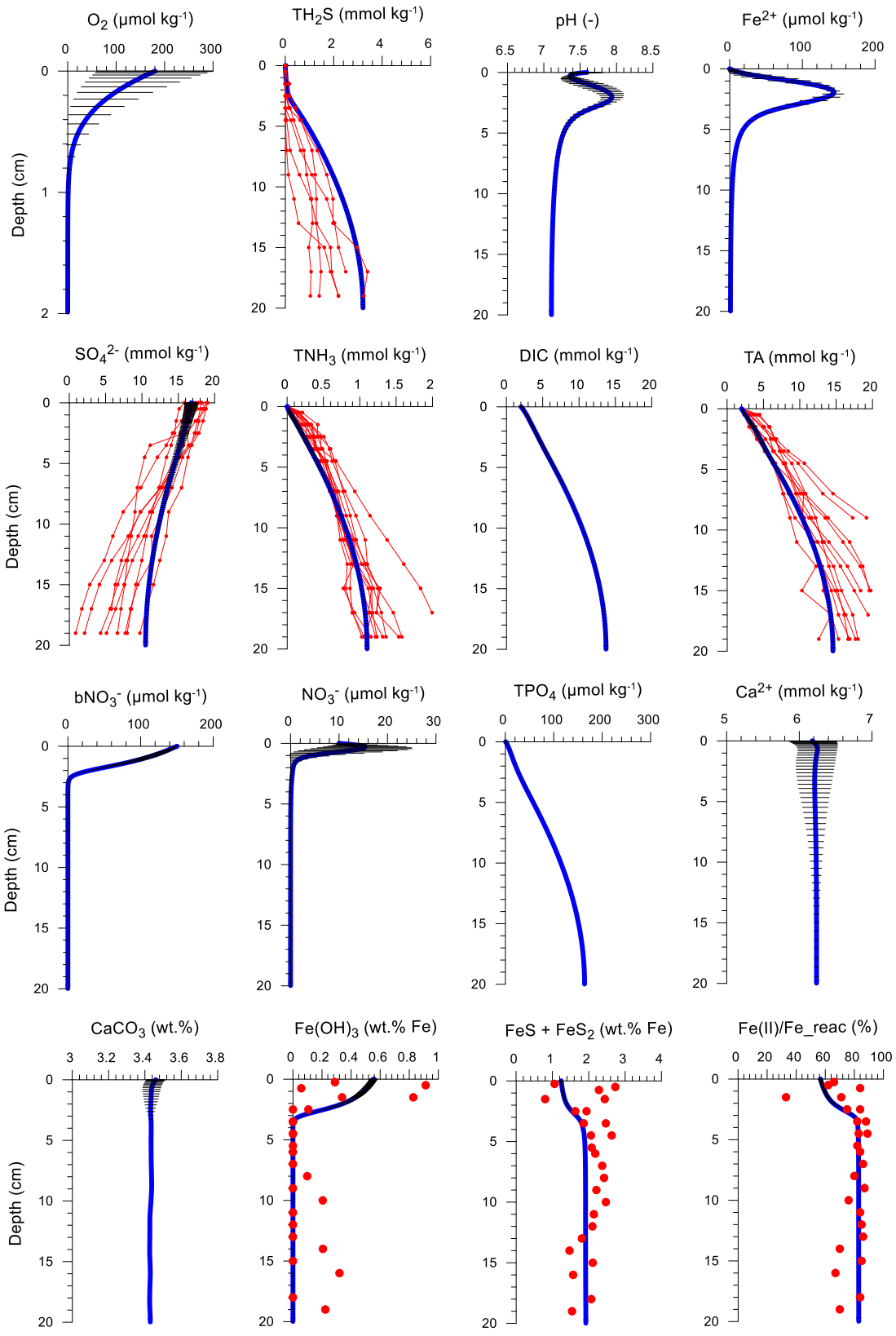

Supplementary Figure 2*. Mean annual (solid blue curves) and standard deviation (black horizontal bars) of modelled geochemistry before mineral addition. Red curves and symbols show the data used to constrain the model. Black horizontal bars on the model curves show the extent of seasonal variability.*

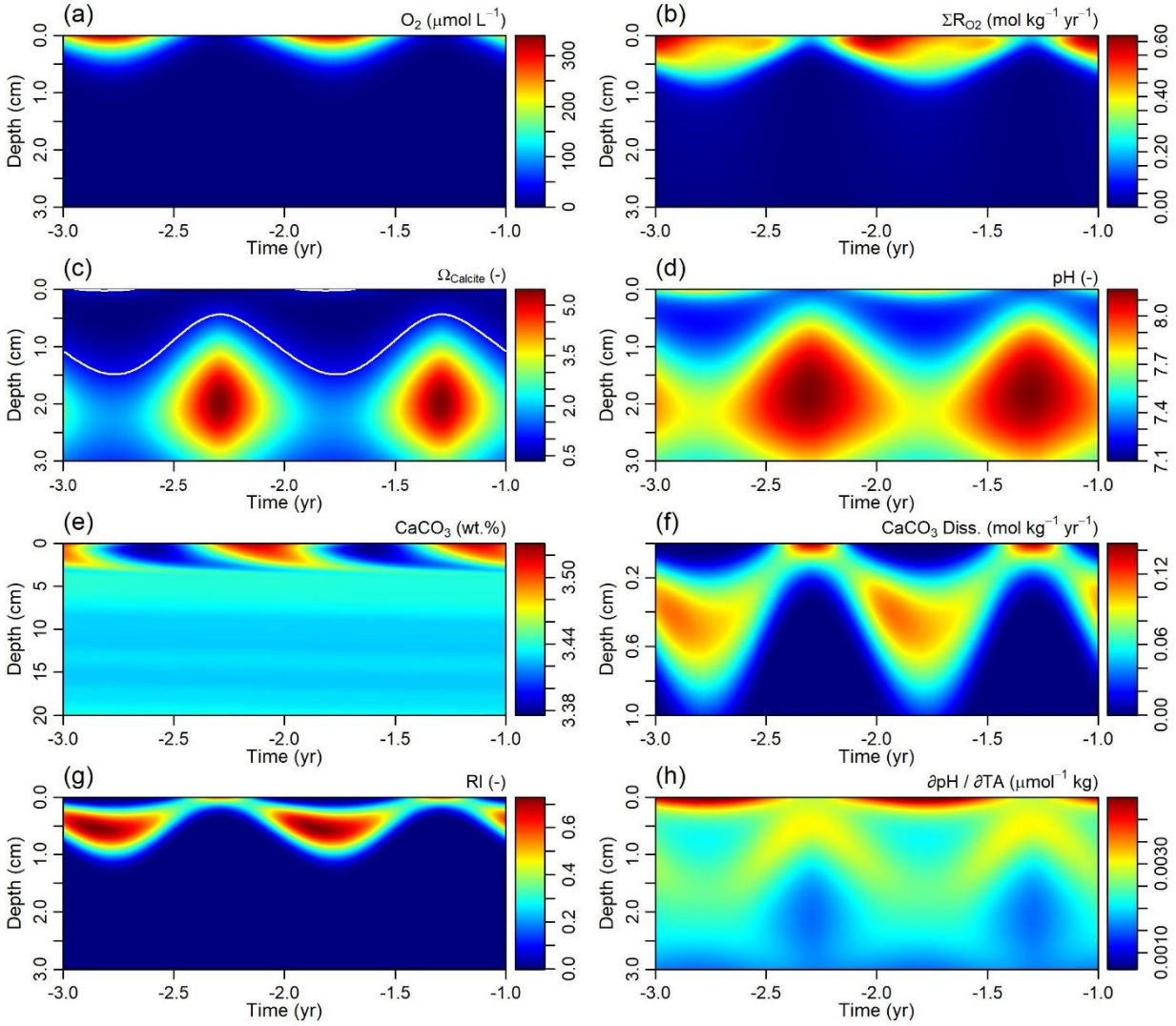

Supplementary Figure 3. *Model results of benthic biogeochemistry for Boknis Eck, SW Baltic Sea prior to calcite addition. The x-axis shows time in years relative to artificial calcite addition beginning year zero. Calendar years begin on 1 January. (a) O_2 concentration, (b) total rate of oxygen consumption, (c) calcite saturation state, (d) pH, (e) calcite content, (f) calcite dissolution rate, (g) respiratory index (carbonate dissolution ÷ POC degradation), (h) sensitivity factor of pH to changes in TA. The white line in (c) denotes $\Omega_{Calcite} = 1$. Note the different depth scales for $CaCO_3$ and calcite dissolution.*

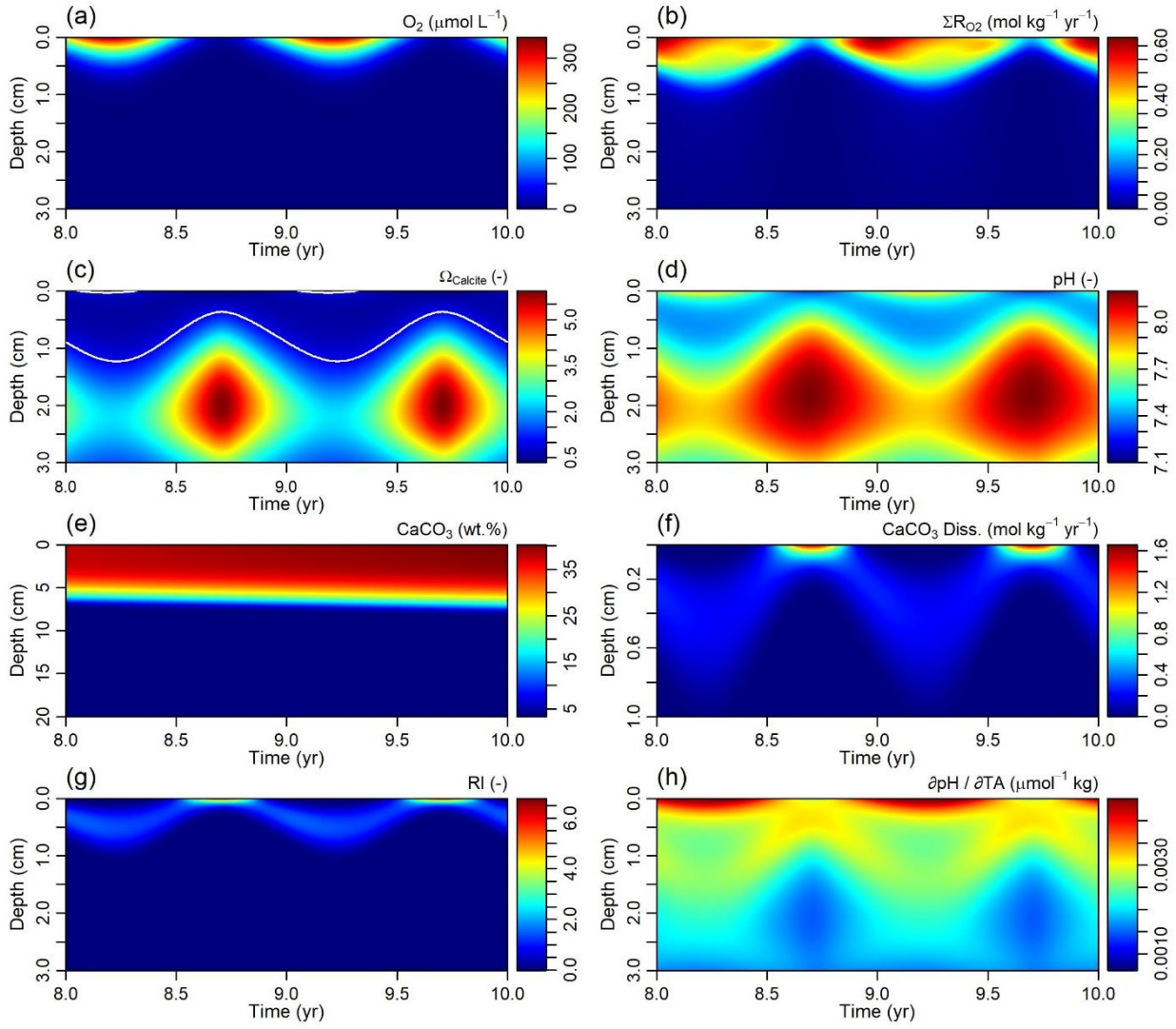

Supplementary Figure 4*. Model results of benthic biogeochemistry for Boknis Eck, SW Baltic Sea, during the final two years of the simulation. The x-axis shows time in years relative to artificial calcite addition beginning year zero. Calendar years begin on 1 January. (A) O_2 concentration, (B) total rate of oxygen consumption, (C) calcite saturation state, (D) pH, (E) calcite content, (F) calcite dissolution rate, (G) respiratory index (carbonate dissolution ÷ POC degradation), (H) sensitivity factor of pH to changes in TA. The white line in (C) denotes $\Omega_{Calcite} = 1$. Note the different depth scales for $CaCO_3$ and calcite dissolution.*

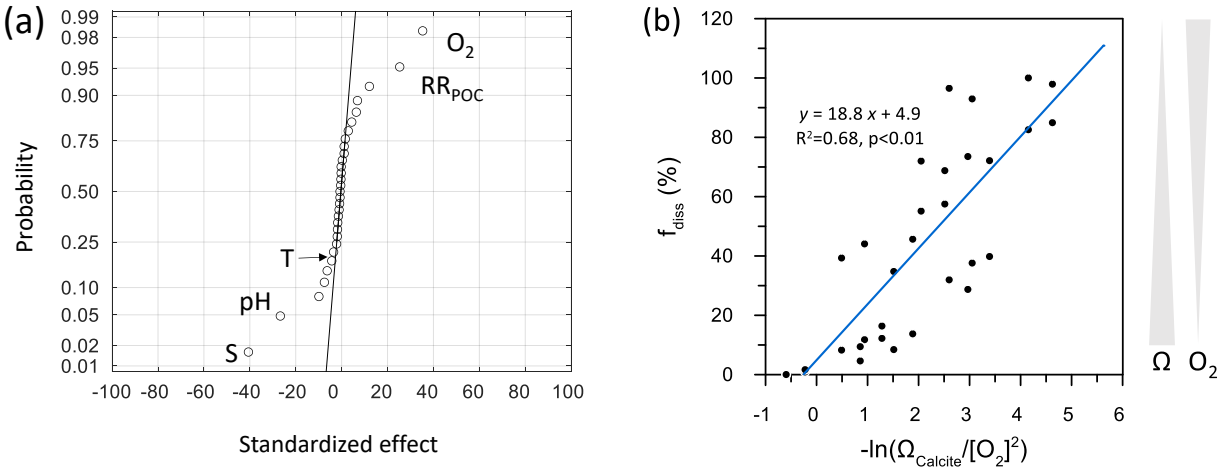

Supplementary Figure 5. *(a) Normal probability plots for calcite dissolution derived from the factorial analysis. Symbols represent 32 possible combinations of the five parameters. The main effects of the tested parameters are indicated next to the respective symbols. For the range of parameters tested, calcite dissolution is most sensitive to the parameters lying away from the normal line, in this case bottom water oxygen concentration and salinity. An increase in the parameter values on the right-hand side of the line (O_2, RR_{POC}) lead to an increase in calcite dissolution. An increase in S and pH has the opposite effect. (b) Fraction of calcite dissolved at Boknis Eck (in %) versus a derived function of calcite saturation and bottom water dissolved oxygen. The results are taken from the sensitivity analysis. The linear fit to the data and corresponding equation is shown. The grey triangles on the right illustrate that f_{diss} is increased by low $\Omega_{Calcite}$ and high O_2 concentrations.*

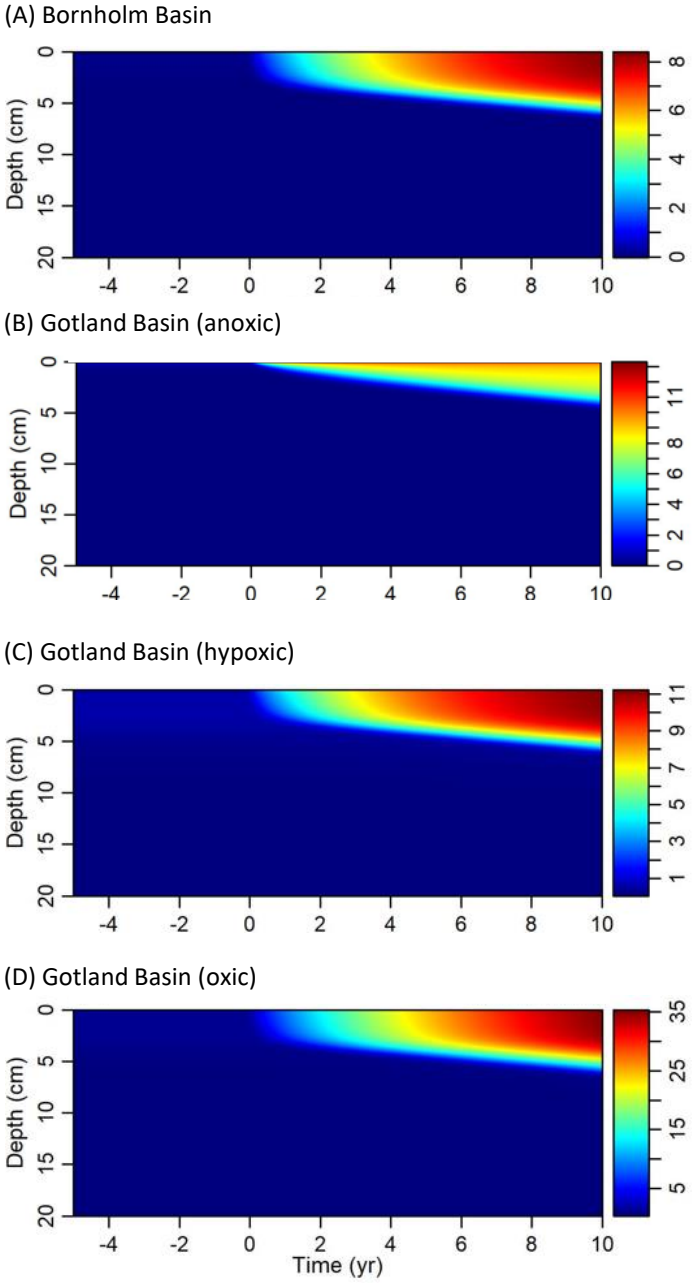

Supplementary Figure 6*. Model results of calcite content for (A) Bothnian Bay and (B)-(D) Gotland Basin. The x-axis shows time in years relative to artificial calcite addition beginning year zero. Calendar years begin on 1 January.*

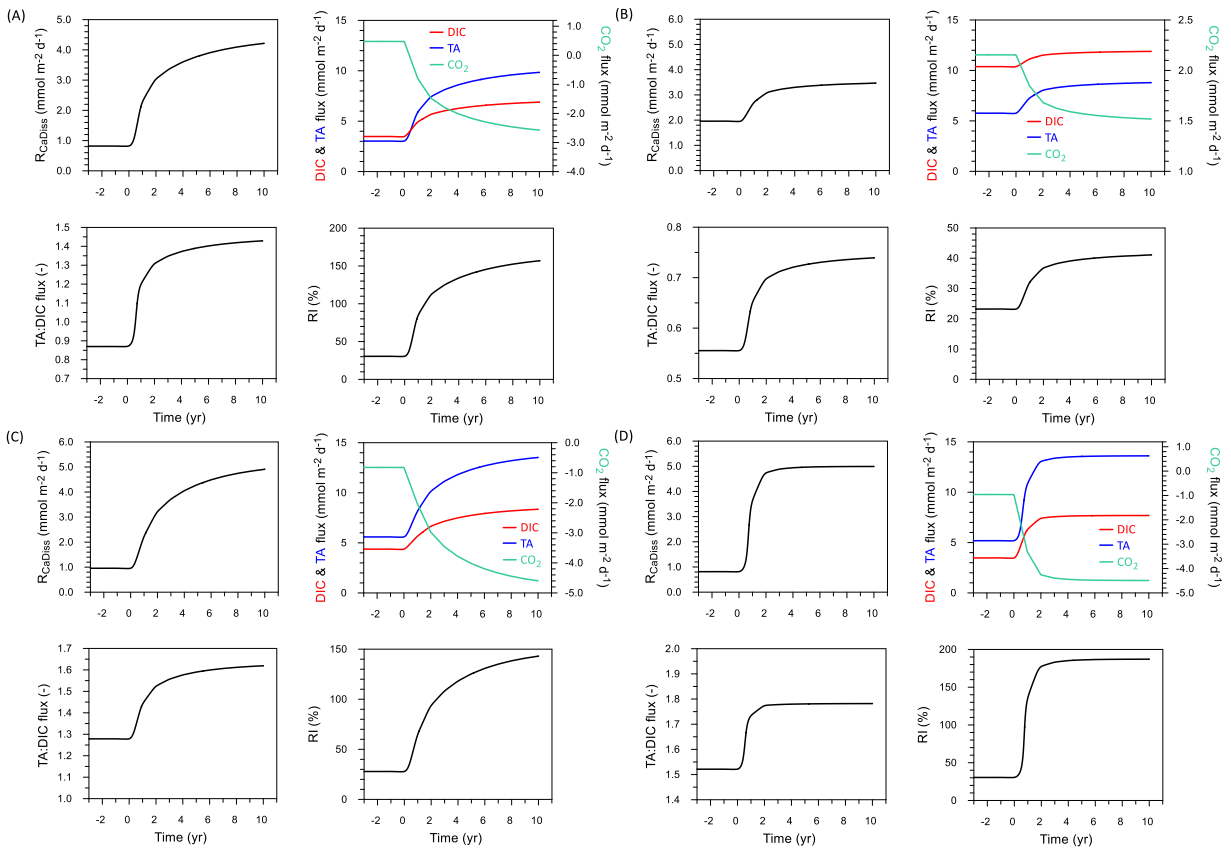

Supplementary Figure 7. *Model results for (A) Bothnian Bay, (B) Gotland Basin oxic, (C) Gotland Basin hypoxic, and (D) Gotland Basin anoxic, including total calcite dissolution rate, benthic fluxes from sediment to the bottom water of DIC, TA and CO_2, TA:DIC flux ratio, and the RI (carbonate dissolution ÷ POC degradation × 100%). The x-axis shows time in years relative to the start of artificial calcite addition beginning year zero.*

Supplementary tables

Supplementary Table 1. Reaction network used in the sediment model.

Stoichiometry	**Rate expression** [a]	**ΔTA**	**ΔDIC**
Particulate organic carbon (POC) degradation [c]			
Rate of POC degradation, R_{POC}	$R_{POC} = \begin{cases} 0.5 \cdot (x + B_1)^{B_2} \text{ for } x \leq 6 \\ 0.5 \cdot (8 + B_1)^{B_2} \text{ for } x > 6 \end{cases}$		+1
POC degradation by oxygen reduction, R_{O2POC}: $CH_2O(NH_3)_{rNC}(PO_4)_{rPC} + O_2 \rightarrow CO_2 + r_{NC}NH_3 + r_{PC}H_3PO_4 + H_2O$	$R_{O2POC} = R_{POC1} \cdot \frac{[O_2]}{[O_2]+K_{O2POC}}$	$r_{NC} - r_{CP}$	+1
POC degradation by denitrification, R_{NO3POC}: $CH_2O(NH_3)_{rNC}(PO_4)_{rPC} + 0.8NO_3^- \rightarrow CO_2 + r_{NC}NH_3 + r_{PC}H_3PO_4 + 0.4N_2 + 1.4H_2O$	$R_{NO3POC} = R_{POC1} \cdot \frac{K_{O2POC}}{[O_2]+K_{O2POC}} \cdot \frac{[NO_3^-]}{[NO_3^-]+K_{KNO3POC}}$	$0.8 + r_{NC} - r_{CP}$	+1
POC degradation by sulphate reduction, R_{SO4POC}: $CH_2O(NH_3)_{rNC}(PO_4)_{rPC} + 0.5SO_4^{2-} \rightarrow CO_2 + 0.5H_2S + r_{NC}NH_3 + r_{PC}H_3PO_4 + H_2O$	$R_{SO4POC} = R_{POC} \cdot \frac{K_{O2POC}}{[O_2]+K_{O2POC}} \cdot \frac{K_{KNO3POC}}{[NO_3^-]+K_{KNO3POC}} \cdot \frac{[SO_4^{2-}]}{[SO_4^{2-}]+K_{SO4POC}}$	$1 + r_{NC} - r_{CP}$	+1
POC degradation by methanogenesis, R_{CH4POC}: $CH_2O(NH_3)_{rNC}(PO_4)_{rPC} \rightarrow 0.5CO_2 + 0.5CH_4 + r_{NC}NH_3 + r_{PC}H_3PO_4$	$R_{CH4POC} = R_{POC} \cdot \frac{K_{O2POC}}{[O_2]+K_{O2POC}} \cdot \frac{K_{KNO3POC}}{[NO_3^-]+K_{KNO3POC}} \cdot \frac{K_{SO4POC}}{[SO_4^{2-}]+K_{SO4POC}}$	$r_{NC} - r_{CP}$	+0.5
Secondary redox reactions			
Aerobic sulphide oxidation, R_{TH2SO2}: $H_2S + 2O_2 \rightarrow SO_4^{2-} + 2H^+$	$R_{H2SO2} = k_{H2SO2} \cdot [TH_2S] \cdot [O_2]$	-2	0
Aerobic iron oxidation, R_{Fe2O2}: $Fe^{2+} + 0.25\ O_2 + 2.5H_2O \rightarrow Fe(OH)_3 + 2H^+$	$R_{Fe2O2} = k_{Fe2O2} \cdot [Fe^{2+}] \cdot [O_2]$	-2	0
Aerobic ammonium oxidation, R_{TNH3O2}: $NH_3 + 2O_2 \rightarrow NO_3^- + H_2O + H^+$	$R_{TNH3O2} = k_{TNH3O2} \cdot [TNH_3] \cdot [O_2]$	-2	0
Anaerobic ammonium oxidation, $R_{TNH3NO3}$: $5/3NH_3 + NO_3^- + H^+ \rightarrow 4/3N_2 + 3H_2O$	$R_{TNH3NO3} = k_{TNH3NO3} \cdot [TNH_3] \cdot [NO_3^-]$	-⅔	0
Anaerobic sulphide oxidation, $R_{TH2SbNO3}$: $H_2S + bNO_3^- + H_2O \rightarrow SO_4^{2-} + NH_3 + H^+$	$R_{TH2SbNO3} = k_{TH2SbNO3} \cdot [TH_2S] \cdot [bNO_3^-]$	0	0
Anaerobic oxidation of methane, R_{CH4SO4}: $SO_4^{2-} + CH_4 + 2H^+ \rightarrow H_2S + CO_2 + 2H_2O$	$R_{CH4SO4} = k_{CH4SO4} \cdot [CH_4] \cdot [SO_4^{2-}]$	+2	+1
Pyrite formation, $R_{TH2SFe(OH)3}$: $2Fe(OH)_3 + 2H_2S + 2H^+ \rightarrow FeS_2 + Fe^{2+} + 6H_2O$	$R_{TH2SFe(OH)3} = k_{TH2SFe(OH)3} \cdot [TH_2S] \cdot [Fe(OH)_3]$	+2	0

Aerobic pyrite oxidation, R_{FeS2O2}: $FeS_2 + 3.5O_2 + H_2O \rightarrow Fe^{2+} + 2SO_4^{2-} + 2H^+$	$R_{FeS2O2} = k_{FeS2O2} \cdot [FeS_2] \cdot [O_2]$	-4	0
Aerobic iron mono-sulphide oxidation, R_{FeSO2}: $FeS + 2.25O_2 + 2.5H_2O \rightarrow Fe(OH)_3 + SO_4^{2-} + 2H^+$	$R_{FeSO2} = k_{FeSO2} \cdot [FeS] \cdot [O_2]$	-2	0
Mineral precipitation and dissolution			
Calcite precipitation $Ca^{2+} + HCO_3^- \rightarrow CaCO_3 + H^+$	$R_{CaPrec} = k_{CaPrec} \cdot (\Omega_{Calcite} - 1)$	-2	-1
Calcite dissolution $CaCO_3 + H^+ \rightarrow Ca^{2+} + HCO_3^-$	$R_{CaDiss} = f_T \cdot k_{CaDiss} \cdot CaCO_3 \cdot (1 - \Omega_{Calcite})^{np}$	+2	+1
Iron mono-sulphide precipitation $Fe^{2+} + HS^- \rightarrow FeS + H^+$	$R_{FeSPrec} = k_{FeSPrec} \cdot [TH_2S] \cdot [Fe^{2+}] \cdot (\Omega_{FeS} - 1)^{nFe}$	-2	0
Iron mono-sulphide dissolution $FeS + H^+ \rightarrow Fe^{2+} + HS^-$	$R_{FeSDiss} = k_{FeSDiss} \cdot [FeS] \cdot (1 - \Omega_{FeS})$	+2	0
Equilibrium reactions			
Carbon dioxide dissociation: $CO_2 + H_2O \rightarrow HCO_3^- + H^+$	$K_1 = \frac{[HCO_3^-] \cdot [H^+]}{[CO_2]}$		
Bicarbonate dissociation: $HCO_3^- \rightarrow CO_3^{2-} + H^+$	$K_2 = \frac{[CO_3^{2-}] \cdot [H^+]}{HCO_3^-}$		
Borate dissociation: $B(OH)_3 + H_2O \rightarrow B(OH)_4^- + H^+$	$K_B = \frac{[B(OH)_4^-] \cdot [H^+]}{B(OH)_3}$		
Ammonium dissociation: $NH_4^+ \rightarrow NH_3 + H^+$	$K_N = \frac{[NH_3] \cdot [H^+]}{NH_4^+}$		
Phosphoric acid dissociation: $H_3PO_4 \rightarrow H_2PO_4^- + H^+$	$K_{P1} = \frac{[H_2PO_4^-] \cdot [H^+]}{[H_3PO_4]}$		
Dihydrogen phosphate dissociation: $H_2PO_4^- \rightarrow HPO_4^{2-} + H^+$	$K_{P2} = \frac{[HPO_4^{2-}] \cdot [H^+]}{[H_2PO_4^-]}$		
Hydrogen phosphate dissociation: $HPO_4^{2-} \rightarrow PO_4^{3-} + H^+$	$K_{P3} = \frac{[PO_4^{3-}] \cdot [H^+]}{[HPO_4^{2-}]}$		
Sulphide dissociation: $H_2S \rightarrow HS^- + H^+$	$K_S = \frac{[HS^-] \cdot [H^+]}{[H_2S]}$		
Water dissociation: $H_2O \rightarrow OH^- + H^+$	$K_W = [OH^-] \cdot [H^+]$		

Supplementary Table 2. Model parameters for the baseline Boknis Eck sediment simulation.

Term	Description	Value	Reference
L	Length of simulated sediment column (cm)	20	1
t_{max}	Simulation time (yr)	1000	1
t_{Ca}	Years of artificial calcite addition (yr)	10	1
T_{mean}	Seasonal temperature amplitude (°C)	7	2
T_{amp}	Mean bottom water temperature (°C)	5	2
S_{mean}	Mean bottom water salinity (-)	21	2
S_{amp}	Seasonal salinity amplitude (-)	1.5	2
O_{2mean}	Mean bottom water oxygen (mmol g^{-1})	0.18	2
O_{2amp}	Seasonal bottom water oxygen amplitude (mmol g^{-1})	0.16	2
pH_{mean}	Mean bottom water pH (-)	7.59	2
pH_{amp}	Seasonal pH amplitude (-)	0.3	2
P	Pressure at seafloor (bar)	4	1
ρ	Dry sediment density (g cm^{-3})	2.5	3
P0	Porosity at sediment surface (–)	0.9	3
Pf	Porosity in compacted sediment (–)	0.8	3
Px	Porosity attenuation length (cm)	0.2	3
ω_{acc}	Burial velocity of compacted sediment (cm yr^{-1})	0.4	3,4
$D_{Bio}0$	Bioturbation coefficient at sediment surface (cm^2 yr^{-1})	30	3
x_{Bio}	Bioturbation depth coefficient (cm)	1	3
α_1	Bioirrigation coefficient at x=0 (yr^{-1})	150 [a]	3
α_2	Bioirrigation depth coefficient (cm)	1	3
α_{N1}	Transport coefficient of biological nitrate at x=0 (yr^{-1})	100	3
Q_{10}	Rate dependency on temperature (-)	2	3
MAR	Mass accumulation rate (g cm^2 yr^{-1})	$\rho\cdot(1-Pf)\cdot u_f$	1
C_{Fe}	Total iron content of sediments (g g^{-1})	0.03	5
AW_{POC}	Atomic weight of POC (g mol^{-1})	12	1
AW_{Fe}	Atomic weight of Fe (g mol^{-1})	55.8	1
AW_{FeS2}	Atomic weight of FeS2 (g mol^{-1})	119.8	1
AW_{FeS}	Atomic weight of FeS (g mol^{-1})	87.8	1
AW_{CaCO3}	Atomic weight of $CaCO_3$ (g mol^{-1})	100	1
RR_{POC}	Mean annual POC rain rate to seafloor (mmol cm^{-2} yr^{-1})	0.438	3
k_{H2SO2}	Rate constant for TH_2S oxidation by O_2 ($mmol^{-1}$ g yr^{-1})	$1\cdot10^8$	3
k_{Fe2O2}	Rate constant for Fe^{2+} oxidation by O_2 ($mmol^{-1}$ g yr^{-1})	$1\cdot10^8$	3
k_{TNH3O2}	Rate constant for TNH_3 oxidation by O_2 ($mmol^{-1}$ g yr^{-1})	$1\cdot10^8$	3
$k_{TNH3NO3}$	Rate constant for TNH_3 oxidation by NO_3^- ($mmol^{-1}$ g yr^{-1})	$1\cdot10^6$	1
$k_{TH2SbNO3}$	Rate constant for TH_2S oxidation by bNO_3^- ($mmol^{-1}$ g yr^{-1})	$1\cdot10^6$	1
k_{CH4SO4}	Rate constant for CH_4 oxidation by SO_4^{2-} ($mmol^{-1}$ g yr^{-1})	$1\cdot10^5$	1
$k_{TH2SFe(OH)3}$	Rate constant for TH_2S oxidation by $Fe(OH)_3$ (g Fe^{-1} g yr^{-1})	$1\cdot10^5$	1
k_{FeS2O2}	Rate constant for FeS_2 oxidation by O_2 (g FeS_2^{-1} g yr^{-1})	100	1
k_{FeSO2}	Rate constant for FeS oxidation by O_2 (g FeS^{-1} g yr^{-1})	$1\cdot10^6$	1
k_{CaPrec}	Rate constant for calcite precipitation ($mmol^{-1}$ g yr^{-1})	0	1
k_{CaDiss}	Rate constant for calcite dissolution (yr^{-1})	See main manuscript	
$k_{FeSPrec}$	Rate constant for FeS precipitation ($mmol^{-1}$ g yr^{-1})	10	1
$k_{FeSDiss}$	Rate constant for FeS dissolution (yr^{-1})	0.3	1
K_{O2POC}	Half–saturation constant for O_2 (mmol g^{-1})	$1\cdot10^{-5}$	1
K_{NO3POC}	Half–saturation constant for NO_3^- (mmol g^{-1})	$1\cdot10^{-5}$	1
K_{SO4POC}	Half–saturation constant for SO_4^{2-} (mmol g^{-1})	$5\cdot10^{-4}$	1
K_{O2Bio}	Half–saturation constant for O_2 for faunal activity (mmol g^{-1})	$2\cdot10^{-5}$	1
B_1	POC degradation rate constant (cm)	1.56	1
B_2	POC degradation rate constant (-)	-1.8	1
r_{NC}	Atomic N-to-C ratio in organic matter (mol N (mol C)$^{-1}$)	16/106	1
r_{PC}	Atomic P-to-C ratio in organic matter (mol P (mol C)$^{-1}$)	1/106	1
np	Reaction order for calcite dissolution	See main manuscript	
nFe	Reaction order for FeS precipitation	2	1
f_{FeHR}	Fraction of reactive Fe that is highly reactive	0.68	1
f_{FeMR}	Fraction of reactive Fe that is moderately reactive	0.13	1

pK_1	Equilibrium constant for CO_2 dissociation (mol kg^{-1})	6.141	6
pK_2	Equilibrium constant for HCO_3^- dissociation (mol kg^{-1})	9.453	6
pK_S	Equilibrium constant for H_2S dissociation (mol kg^{-1})	6.894	6
pK_B	Equilibrium constant for $B(OH)_3$ dissociation (mol kg^{-1})	8.954	6
pK_N	Equilibrium constant for NH_4^+ dissociation (mol kg^{-1})	9.909	6
pK_{P1}	Equilibrium constant for H_3PO_4 dissociation (mol kg^{-1})	1.701	6
pK_{P2}	Equilibrium constant for $H_2PO_4^-$ dissociation (mol kg^{-1})	6.267	6
pK_{P3}	Equilibrium constant for HPO_4^{2-} dissociation (mol kg^{-1})	9.339	6
pK_W	Equilibrium constant for H_2O dissociation (mol kg^{-1})[2]	14.130	6
pK_0	Solubility constant for CO_2 (mol kg^{-1} atm^{-1})	1.278	6
pK_{sp}	Solubility product of $CaCO_3$ (mol kg^{-1})[2]	6.614	6
K_{FeS}	Solubility product of FeS (mol kg^{-1})	0.00316	7

[a] Irrigation coefficients for TH_2S and Fe^{2+} were set to zero to simulate particulate iron sulphide contents.
[1] This study; [2] Melzner et al.[17]; [3] Dale et al.[1]; [4] Dale et al.[20]; [5] Perner et al.[15]; [6] Zeebe and Wolf-Gladrow[5], on free scale where appropriate; [7] Meysman et al.[21];

Supplementary Table 3. Depth–dependent constitutive equations.

Parameter	Equation
Porosity	$\varphi = Pf + (P0 - Pf) \cdot \exp(-px \cdot x)$
Molecular diffusion [a]	$D_S = \frac{D_W}{1-\ln(\varphi^2)}$
Burial velocity of solids	$u_s = \frac{(1-Pf)\cdot\omega_{acc}}{(1-\varphi)}$
Burial velocity of porewater	$u_{pw} = \frac{Pf\cdot\omega_{acc}}{\varphi}$
Bioturbation	$D_B = D_{Bio}0 \cdot \exp\left(-\frac{x^2}{2\cdot {x_{Bio}}^2}\right) \cdot \left(\frac{bw[O2]}{K_{O2Bio}+bw[O2]}\right)$
Bioirrigation	$\alpha = \alpha_1 \cdot \exp\left(-\frac{\alpha_2 - x}{1+\exp(\alpha_2 - x)}\right) \cdot \left(\frac{bw[O2]}{K_{O2Bio}+bw[O2]}\right)$
Non-local biological NO_3^- transport	$\alpha = \alpha_{N1} \cdot \exp(-0.5 \cdot x^2)$
Temperature rate dependency	$f_T = Q_{10}^{\frac{T-T_{ref}}{10}}$
Conversion factor between solid and dissolved species [b]	$f_S = \frac{\rho\cdot(1-Pf)\cdot 10^3}{\varphi\cdot\rho_{SW}\cdot AW}$
Saturation state of calcite	$\Omega_{Calcite} = \frac{[Ca^{2+}]\cdot[CO_3^{2-}]}{K_{sp}}$
Saturation state of iron mono-sulphide	$\Omega_{FeS} = \frac{[Fe^{2+}]\cdot[HS^-]}{[H^+]\cdot K_{FeS}}$

[a] Molecular diffusion coefficients in water (D_W) were mostly taken from Boudreau[22] and depend on bottom water temperature and salinity. The diffusion coefficient for bNO_3^- was set to a low value (10^{-6}) since nitrate stored inside large sulphur bacteria is assumed to be transported by non-local pathways[1].
[b] Seawater density (ρ_{sw}) was calculated as function of temperature and salinity[5].

Supplementary Table 4. Boundary conditions at the sediment surface [a].

Variable	**Value**
$Fe(OH)_3$ (g Fe cm^{-2} yr^{-1})	$MAR \cdot C_{Fe} \cdot f_{FeHR}$
Fe_{MR} (g Fe cm^{-2} yr^{-1})	$MAR \cdot C_{Fe} \cdot f_{FeMR}$
FeS_2 (g FeS_2 cm^{-2} yr^{-1})	0
FeS (g FeS cm^{-2} yr^{-1})	0
$CaCO_3$ (g $CaCO_3$ cm^{-2} yr^{-1}) [b]	$2 \cdot \frac{AW_{CaCO_3}}{AW_{POC}} \cdot RR_{POC} \cdot \left(1 - \frac{1}{1+\exp\left(\frac{t-t_{max}+t_{Ca}}{0.03}\right)} + \frac{AW_{POC}}{AW_{CaCO_3}}\right)$
O_2 (mmol g^{-1})	Eq. (24)
SO_4^{2-} (mmol g^{-1})	$0.028 \cdot bw[S]/35$
TH_2S (mmol g^{-1})	0
TNH_3 (mmol g^{-1})	$1 \cdot 10^{-5}$
TPO_4 (mmol g^{-1})	$1 \cdot 10^{-6}$
Fe^{2+} (mmol g^{-1})	0
Ca^{2+} (mmol g^{-1})	$0.0103 \cdot bw[S]/35$
DIC (mmol g^{-1})	Eq. (43)
TB (mmol g^{-1})	$416 \cdot 10^{-6} \cdot bw[S]/35$
H^+ (mmol g^{-1})	Eq. (27)
CH_4 (mmol g^{-1})	0
NO_3^- (mmol g^{-1})	$1 \cdot 10^{-5}$
bNO_3^- (mmol g^{-1})	$15 \cdot 10^{-4}$

[a] All lower boundaries are defined with a Neumann condition equal to zero.
[b] RR_{POC} is in g cm^{-2} yr^{-1}

Supplementary Table 5. Parameter values for the model simulations of Bothnian Bay and the eastern Gotland Basin sediments. These simulations employed constant boundary conditions. Also shown are the derived values of bottom water calcite saturation state for the given conditions. Mean annual values for Boknis Eck from this study are shown for comparison.

	Bothnian Bay (St. F9/A13)	GB (oxic)	GB (hypoxic)	GB (anoxic)	Boknis Eck
Sed. Rate (cm yr^{-1})	0.25 [a]	0.25 [a,b]	0.25 [a,b]	0.25 [a,b]	0.4
RR_{POC} (g C m^{-2} yr^{-1})	15 [c]	38 [d]	18 [d]	15 [d]	53
RR_{CaCO3} (g $CaCO_3$ m^{-2} yr^{-1}) †	250	633	300	250	875
f_{FeHR} (–)	0.3	0.3	0.3	0.3	0.68
$bw[O_2]$ (µmol kg^{-1})	300 [e]	300 [d]	20 [d]	0 [d]	180
$bw[NO_3^-]$(µmol kg^{-1})	8 [e]	2 [d]	7 [d]	0 [d]	10
$bw[bNO_3^-]$ (µmol kg^{-1})	0 [f]	0 [f]	150 [f]	0 [f]	150
$bw[NH_4^+]$ (µmol kg^{-1})	1 [e]	1 [d]	2 [d]	20 [d]	10
$bw[TPO_4]$ (µmol kg^{-1})	1 [g]	1 [d]	3 [d]	5 [i]	1
$bw[TH_sS]$ (µmol kg^{-1})	0 [g]	0 [d]	0 [d]	90 [i]	0
bw[S] (–)	3.8 [h]	7 [i]	10 [i]	13 [i]	21
bw[T] (^oC)	2.2 [h]	10 [i]	6 [i]	6 [i]	7
bw[pH] (–)	7.53 [h,j]	8.10 [i,j]	7.19 [i,j]	7.14 [i,j]	7.7
bw[TA] (µmol kg^{-1})	993 [h]	1650 [i]	1750 [i]	1950 [i]	2000
Ω_{Ca} (–)	0.13	1.22	0.30	0.23	0.92

† Rain rate of artificial calcite

[a] Mattila et al.[23]; [b] Christiansen and Kunzendorf[24]; [c] Leipe et al.[25]; [d] Noffke et al.[26]; [e] Stockenberg and Johnstone[27]; [f] This study; [g] Assumed equal to GB oxic; [h] Downloaded from the Swedish Ocean Archive (SHARK) database provided by the Swedish Meteorological and Hydrological Institute (SMHI; http://sharkweb.smhi.se/, last access: September 2023). [i] Ulfsbo et al.[18]; [j] NBS scale. These were converted to the free scale using Eq. (2) in Ulfsbo et al.[18] and dissociation constants for HSO_4^- and HF reported by Zeebe and Wolf-Gladrow[5].

Supplementary Table 6. Fluxes of acid-base species and TA at the sediment surface prior to addition of calcite. The net TA flux to the bottom water is balanced by the net rate of TA production presented in Table 1 (main manuscript). Positive fluxes are from the sediment to the bottom water and vice versa.

Species	Contribution to TA	Flux ($\mu mol\ cm^{-2}\ yr^{-1}$)	TA Flux ($\mu mol\ cm^{-2}\ yr^{-1}$)	
CO_2	0	79.6	0.0	
HCO_3^-	1	410.4	410.4	
CO_3^{2-}	2	-20.7	-41.4	
$B(OH)_4^-$	1	-10.3	-10.3	
$B(OH)_3$	0	10.2	0.0	
H_2S	0	1.6	0.0	
HS^-	1	5.7	5.7	
OH^-	1	-1.5	-1.5	
NH_3	1	0.2	0.2	
NH_4^+	0	36.7	0.0	
H_3PO_4	-1	0.0	0.0	
$H_2PO_4^-$	0	0.2	0.0	
HPO_4^{2-}	1	3.8	3.8	
PO_4^{3-}	2	0.1	0.1	
H^+	-1	0.1	-0.1	
		Sum	366.9	$\mu mol\ cm^{-2}\ yr^{-1}$
			10.1	$mmol\ m^{-2}\ d^{-1}$

Supplementary Table 7. Reaction rates at Boknis Eck and their contribution to TA after 10 years of calcite addition. Also shown are the irreversible TA sources by sulphide burial, denitrification and calcite dissolution.

	Rate	ΔTA	Rate TA	
	(µmol cm^{-2} yr^{-1})	(see Supp. Table 1)	(µmol cm^{-2} yr^{-1})	
POC degradation by O_2	81.9	0.14	11.6	
POC degradation by NO_3^-	30.7	0.94	28.9	
POC degradation by SO_4^{2-}	313.9	1.14	358.3	
POC degradation by CH_4	11.3	0.14	1.6	
Aerobic NH_4^+ oxidation	33.1	-2	-66.1	
Anaerobic NH_4^+ oxidation	0.5	-0.67	-0.3	
Aerobic H_2S oxidation	10.3	-2	-20.7	
Aerobic Fe^{2+} oxidation	16.4	-2	-32.7	
Anaerobic H_2S oxidation	5.1	0	0.0	
Pyrite formation	53.3	2	106.5	
Aerobic pyrite oxidation	0.1	-2	-0.2	
FeS precipitation	32.3	-2	-64.5	
FeS dissolution	0.1	2	0.3	
Aerobic FeS oxidation	17.1	-2	-34.2	
Anaerobic CH_4 oxidation	5.5	2	10.9	
$CaCO_3$ dissolution	97.3	2	194.6	
$CaCO_3$ precipitation	0.0	-2	0.0	
TA flux at bottom	4.8	-1	-4.8	
		Sum	489.2	µmol cm^{-2} yr^{-1}
		Sum	13.4	mmol m^{-2} d^{-1}
FeS burial	15.0	2	29.9	
FeS_2 burial	53.6	4	214.5	
POC degradation by NO_3^-	30.7	0.94	28.9	
$CaCO_3$ dissolution	97.3	2	194.6	

Supplementary Table 8. Fluxes of acid-base species and TA at the sediment surface after 10 years of artificial calcite addition. Positive fluxes are from the sediment to the bottom water and vice versa.

Species	Contribution to TA	Flux ($\mu mol\ cm^{-2}\ yr^{-1}$)	TA Flux ($\mu mol\ cm^{-2}\ yr^{-1}$)	
CO_2	0	35.2	0.0	
HCO_3^-	1	503.9	503.9	
CO_3^{2-}	2	-8.8	-17.6	
$B(OH)_4^-$	1	-6.2	-6.2	
$B(OH)_3$	0	6.1	0.0	
H_2S	0	1.6	0.0	
HS^-	1	5.7	5.7	
OH^-	1	-1.0	-1.0	
NH_3	1	0.2	0.2	
NH_4^+	0	36.7	0.0	
H_3PO_4	-1	0.0	0.0	
$H_2PO_4^-$	0	0.2	0.0	
HPO_4^{2-}	1	3.8	3.8	
PO_4^{3-}	2	0.1	0.2	
H^+	-1	0.0	0.0	
		Sum	488.8	$\mu mol\ cm^{-2}\ yr^{-1}$
			13.4	$mmol\ m^{-2}\ d^{-1}$